Atmos. Chem. Phys., 16, 8141–8156, 2016
www.atmos-chem-phys.net/16/8141/2016/
doi:10.5194/acp-16-8141-2016

Atmospheric Chemistry and Physics Open Access EGU

New insight into the spatiotemporal variability and source apportionments of C_1–C_4 alkyl nitrates in Hong Kong

Zhenhao Ling[1,2], Hai Guo[2], Isobel Jane Simpson[3], Sandra Maria Saunders[4], Sean Ho Man Lam[4,5], Xiaopu Lyu[2], and Donald Ray Blake[3]

[1]School of Atmospheric Sciences, Sun Yat-sen University, Guangzhou, China
[2]Air Quality Studies, Department of Civil and Environmental Engineering, The Hong Kong Polytechnic University, Hong Kong, Hong Kong
[3]Department of Chemistry, University of California at Irvine, California, USA
[4]School of Chemistry and Biochemistry, University of Western Australia, Perth, Western Australia, Australia
[5]Pacific Environment Limited, Perth, Western Australia, Australia

Correspondence to: Hai Guo (ceguohai@polyu.edu.hk)

Received: 22 June 2015 – Published in Atmos. Chem. Phys. Discuss.: 24 August 2015
Revised: 7 May 2016 – Accepted: 13 June 2016 – Published: 6 July 2016

Abstract. C_1–C_4 alkyl nitrates ($RONO_2$) were measured concurrently at a mountain site, Tai Mo Shan (TMS), and an urban site, Tsuen Wan (TW), at the base of the same mountain in Hong Kong from September to November 2010. Although the levels of parent hydrocarbons were much lower at TMS ($p < 0.05$), similar alkyl nitrate levels were found at both sites regardless of the elevation difference, suggesting various source contributions of alkyl nitrates at the two sites. Prior to using a positive matrix factorization (PMF) model, the data at TW were divided into "meso" and "non-meso" scenarios for the investigation of source apportionments with the influence of mesoscale circulation and regional transport, respectively. Secondary formation was the prominent contributor of alkyl nitrates in the meso scenario (60 ± 2 %, 60.2 ± 1.2 pptv), followed by biomass burning and oceanic emissions, while biomass burning and secondary formation made comparable contributions to alkyl nitrates in the non-meso scenario, highlighting the strong emissions of biomass burning in the inland Pearl River delta (PRD) region. In contrast to TW, the alkyl nitrate levels measured at TMS mainly resulted from the photooxidation of the parent hydrocarbons at TW during mesoscale circulation, i.e., valley breezes, corresponding to 52–86 % of the alkyl nitrate levels at TMS. Furthermore, regional transport from the inland PRD region made significant contributions to the levels of alkyl nitrates ($\sim$ 58–82 %) at TMS in the non-meso scenario, resulting in similar levels of alkyl nitrates observed at the two sites. The simulation of secondary formation pathways using a photochemical box model found that the reaction of alkyl peroxy radicals (RO_2) with nitric oxide (NO) dominated the formation of $RONO_2$ at both sites, and the formation of alkyl nitrates contributed negatively to O_3 production, with average reduction rates of 4.1 and 4.7 pptv pptv^{-1} at TMS and TW, respectively.

1 Introduction

Alkyl nitrates ($RONO_2$) are important photochemical pollutants in the atmosphere because of their roles in local, regional and global atmospheric chemistry (Jenkin and Clemitshaw, 2000; Seinfeld and Pandis, 2006). Alkyl nitrates are reactive nitrogen compounds (NO_y) and act as a critical reservoir of nitrogen oxides ($NO_x = NO + NO_2$) during long-range transport resulting from their relatively low reactivity (Atkinson et al., 2006).

A number of studies conducted in different environments have shown that alkyl nitrates are either emitted from marine sources directly and/or produced indirectly through photochemical reactions (Roberts et al., 1998; Blake et al., 2003; Simpson et al., 2002, 2003, 2006; Reeves et al., 2007; Wang et al., 2013). In the case of biomass burning, secondary alkyl nitrate formation is believed to occur by the photooxidation of emitted hydrocarbons with a formation mechanism of RO

and NO_2 (Simpson et al., 2002). The photochemical pathways for the secondary formation of alkyl nitrates are expressed as follows (Atkinson et al., 2006; Jenkin and Clemitshaw, 2000; Arey et al., 2001; Sommariva et al., 2008):

$$RH + OH^{\bullet} \rightarrow R^{\bullet} + H_2O, k_1, \alpha_1 \quad (R1)$$

$$R^{\bullet} + O_2 \rightarrow RO_2{}^{\bullet}, k_2 \quad (R2)$$

$$RO_2{}^{\bullet} + NO \rightarrow RO^{\bullet} + NO_2, k_3, 1-\alpha_2, \quad (R3)$$

$$RO_2{}^{\bullet} + NO \rightarrow RONO_2, k_4, \alpha_2, \quad (R4)$$

$$RO + NO_2 \rightarrow RONO_2, k_5, \quad (R5)$$

where k_1, k_2, k_3, k_4 and k_5 are reaction rate constants. α_1 and α_2 are branching ratios for the corresponding radicals, which increase as the carbon number increases and are dependent on the carbon chain length.

Photochemical formation of alkyl nitrates influences the oxidation of NO to NO_2, subsequently leading to O_3 production by NO_2 photolysis. Therefore, alkyl nitrates are often used as indicators of photochemical O_3 production (Simpson et al., 2006). Furthermore, the interactions of alkyl nitrates with their parent hydrocarbons provide useful information about the photochemical processing of air masses. Comparing measured and predicted $RONO_2$ / RH ratios calculated using the laboratory kinetic data as a function of time, Bertman et al. (1995) examined the photochemical evolution of alkyl nitrates at Scotia, Pennsylvania and the Kinterbish Wildlife Area, Alabama. Since then, this approach has been used to investigate the evolution of alkyl nitrates with air mass age in different regions (Simpson et al., 2006; Reeves et al., 2007; Russo et al., 2010; Worton et al., 2010; Wang et al., 2013). Fairly good agreement (> 0.5) between measured and modeled ratios suggests that the oxidation of single-parent hydrocarbons represents the evolution of their daughter alkyl nitrates, while poor correlation indicates sources other than the photochemical formation of alkyl nitrates.

In contrast, the main sinks for ambient alkyl nitrates are photolysis and reactions with hydroxyl radical (OH), making alkyl nitrate lifetimes vary with season, latitude and altitude (days to weeks):

$$RONO_2 + h\nu \rightarrow RO^{\bullet} + NO_2, J_{RONO_2}, \quad (R6)$$

$$RONO_2 + OH^{\bullet} \rightarrow \text{products}, k_6, \quad (R7)$$

where $h\nu$ is sunlight and J_{RONO_2} and k_6 are the photolysis and OH reaction rate constants, respectively. The importance of alkyl nitrate removal by photolysis decreases as the carbon number increases (Clemitshaw et al., 1997; Talukdar et al., 1997). Dry deposition has recently been recognized as another pathway for the removal of atmospheric alkyl nitrates (Russo et al., 2010; Wu et al., 2011).

Despite increased concern over photochemical pollution in Hong Kong and the greater Pearl River delta (PRD) region, limited studies have focused on the characteristics of alkyl nitrates, which share a common mechanism with photochemical O_3 formation and act as indicators of photochemical processing. For example, based on measurements conducted in 2001–2002, including during ozone episodes, Simpson et al. (2006) analyzed the general characteristics of alkyl nitrates at a coastal site (Tai O) in Hong Kong. C_3–C_4 alkyl nitrates were the most abundant species, with maximum and minimum levels in winter and summer, respectively. The diurnal variations suggested that photochemical production was the dominant source of alkyl nitrates at Tai O. Furthermore, through approximate calculations, it was concluded that the methoxy radical ($CH_3O^{\bullet}$) reaction with NO_2 was a viable alternative pathway for the observed high levels of $MeONO_2$ during pollution episodes. This mechanism was subsequently verified by Archibald et al. (2007) via box model simulations, whereby $RO + NO_2 \rightarrow RONO_2$ became important for $MeONO_2$ formation at 10 ppb NO_2 and dominant at 35 ppb NO_2. However, knowledge related to the chemical evolution and source apportionments of individual alkyl nitrates and their relationship with parent hydrocarbons is still lacking for Hong Kong, especially given that levels of alkyl nitrate precursors have varied since 2002 (Ling and Guo, 2014). Hence, in this study, intensive field measurements of C_1–C_4 alkyl nitrates were conducted at two sites – a mountain site (Tai Mo Shan, TMS) and an urban site (Tsuen Wan, TW) at the base of the same mountain in Hong Kong. The data were analyzed and compared with the previous study conducted at Tai O (Simpson et al., 2006). The aims were to investigate the spatiotemporal variations and, for the first time, source apportionments and photochemical formation pathways and evolution of alkyl nitrates in Hong Kong.

2 Methodology

2.1 Sampling sites

In this study, concurrent field measurements were conducted at two sites located at different elevations of the highest mountain, Tai Mo Shan (TMS) with an elevation of 957 m a.s.l. in Hong Kong from 6 September to 29 November 2010. A detailed description of the topography of TMS was provided in an overview paper (Guo et al., 2013a). In brief, Fig. 1 presents the two sampling locations and the surroundings. The high-elevation site (TMS) was set on the rooftop of a building on the mountainside (640 m a.s.l.), the highest logistically feasible observation location, beyond which the area comprised the natural landscape with shrubs and grasses to the mountain summit (AFCD, 2008). The measurement site at the base of the mountain was the monitoring station of the Hong Kong Environmental Protection Department (HKEPD) at Tsuen Wan (TW), a mixed residential, commercial and light industrial area in the New Territories of Hong Kong. The TW monitoring site was located on the rooftop of a building, approximately 20 m above ground level. The linear distance between the TMS and TW sites was about 7 km, and the difference in elevation between the

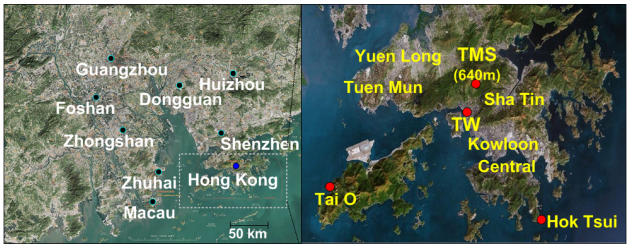

Figure 1. Tai Mo Shan (TMS) and Tsuen Wan (TW) sampling sites and the surrounding environments in Hong Kong.

two sites was 630 m. In general, solar radiation was comparable at the two sites, while the temperature was higher and the relative humidity and wind speed were lower at the TW site (Guo et al., 2013a). The winds at TMS were generally from the north with speeds ranging from 0.02 to 4 m s^{-1}, and the winds at TW were predominantly from the southeast at speeds of 1–3 m s^{-1} with easterly winds at night and southerly winds during the day. Because of its unique topography, the air at TMS was often influenced by the mountain-valley breezes and regional transport (Guo et al., 2013a). Based on the average wind speed of 1.9 m s^{-1}, air masses transported from upwind locations, on both local (∼ 7 km) and regional scales (∼ 20 km), took approximately 1–3 h to arrive at the TMS site (Guo et al., 2012, 2013a).

The Tai O sampling station was a rural–coastal site located on the western coast of Lantau Island in southwestern Hong Kong (elevation, 80 m a.s.l.) (Fig. 1). This site overlooks the Pearl River estuary to the west and north and the South China Sea to the south. It is 32 km away from the urban center to the east and about the same distance from Macau and Zhuhai to the west. Major man-made sources in the region are located to the east, north and southwest. Local emissions are small because of a sparse population and light traffic. Owing to Asian monsoon circulation, this site is frequently affected by polluted continental air masses from the highly industrialized PRD region of mainland China in cold seasons. A detailed description of the site is provided in Wang et al. (2003).

2.2 Sampling and analysis of volatile organic compounds (VOCs)

Whole-air samples were collected on 10 O_3 episode days and 10 non-O_3 episode days using evacuated 2 L stainless steel canisters. Each of the collected canister samples was integrated over a 60 min sampling period. A total of 384 samples were collected at the two sites. The O_3 episode days were selected as the days with the highest daytime hourly O_3 level on a regional scale (higher than 100 ppbv), which were based on weather forecasts and meteorological data analysis, and confirmed by the observed O_3 mixing ratios. During non-O_3 episode days, 1 h integrated samples were collected at 2 h intervals from 07:00 to 19:00 local time (LT) (seven samples per day). On O_3 episode days, 1 h integrated samples were collected from 09:00 to 16:00 LT at 1 h intervals with additional integrated samples collected at 18:00, 21:00, 00:00, 03:00 and 07:00 LT (a total of 13 samples per day). After the campaign, the canister samples were sent to the University of California, Irvine (UCI), for chemical analysis. Other studies have provided detailed descriptions of the analytical system and the quality control, detection limits, and analysis precision of the VOC samples (Simpson et al., 2006, 2010). In brief, the precision and detection limit of the alkyl nitrate measurements are 5 % and 0.02 pptv, respectively. The calibration scale for the alkyl nitrate measurements changed in 2008, increasing by factors of 2.13, 1.81, 1.24 and 1.17 for the C_1, C_2, C_3 and C_4 alkyl nitrates, respectively (Simpson et al., 2011). In other words, the alkyl nitrates reported at Tai O by Simpson et al. (2006) were lower than the data reported here, and the Tai O data have been adjusted to the new calibration scale to allow direct comparison with this work. The Tai O sampling campaign was conducted from 24 August 2001 to 31 December 2002. Different from the air samples collected at TMS and TW, each whole-air sample at Tai O was collected for only 1 min, and was then analyzed at UCI. Intensive sampling from 07:00 to 19:00 LT was conducted every 2 h during the selected pollution episodes (17–19 October 2001, 29–30 August, 5–6 September, 9–11 and 25 October, 6–8 and 12 November 2002). Apart from the intensive sampling days, samples were taken either daily or every few days, typically in the midafternoon (Simpson et al., 2006).

2.3 Continuous measurements of O_3, carbon monoxide (CO) and nitric oxide–nitrogen dioxide–nitrogen oxides (NO–NO_2–NO_x)

At TMS, online measurements of O_3, CO and NO–NO_2–NO_x were made using commercial analyzers. Ozone was measured using a commercial UV photometric instrument (Advanced Pollution Instrumentation (API), model 400E) that has a detection limit of 0.6 ppbv. Carbon monoxide was measured with a gas filter correlation, nondispersive infrared analyzer (API, Model 300E) with a heated catalytic scrubber (as purchased) to convert CO to carbon dioxide (CO_2) for background determination. The detection limit was 30 ppbv for a 2 min average. The 2σ precision was about 1 % for a level of 500 ppbv (2 min average) and the overall uncertainty was estimated to be 10 %. NO, NO_2 and NO_x were detected with a chemiluminescence NO–NO_2–NO_x analyzer (API, Model 200E) that had a detection limit of 0.5 ppbv. The O_3 analyzer was calibrated weekly by using a transfer standard (Thermo Environmental Instruments (TEI) 49 PS), while the other analyzers were zeroed daily by analyzing scrubbed ambient air and calibrated weekly by a span gas mixture with a NIST (National Institute of Standards and Technology) traceable standard, which was diluted to representative mixing ratios using a dynamic calibrator (Envi-

ronics, Inc., Model 6100). The Standard (Scott-Marrin, Inc.) contained 156.5 ppmv CO (±2 %), 15.64 ppmv SO_2 (±2 %) and 15.55 ppmv NO (±2 %). For the O_3, CO and NO–NO_2–NO_x analyzers; a data logger (Environmental Systems Corporation Model 8816) was used to control the calibrations and to collect 1 min data.

In addition to the above chemical measurements, several meteorological parameters, including wind speed and direction, temperature, relative humidity and solar radiation, were measured by the integrated sensor suite (Vantage Pro TM & Vantage Pro 2 Plus TM Weather Stations, Davis Instruments).

At TW, hourly O_3, CO, NO–NO_2–NO_x and meteorological data were obtained from the HKEPD (http://epic.epd.gov.hk/ca/uid/airdata). The hourly data were subsequently derived by averaging 1 min data over the same time interval as the TMS data. Detailed information about the measurements, quality assurance and control protocols can be found in the HKEPD report (HKEPD, 2012). In addition, Table S1 in the Supplement shows descriptive statistics of the main non-methane hydrocarbons (NMHCs) and trace gases at both sites, while Fig. S1 presents the time series of trace gases and meteorological parameters at the two sites.

2.4 Positive matrix factorization (PMF) model

In this study, the US EPA PMF 3.0 (https://www.epa.gov/air-research/models-tools-and-databases-air-research) was used for the source apportionments of the observed alkyl nitrates at TW. Our previous studies provided detailed information about the PMF model (Ling et al., 2011; Ling and Guo, 2014). In terms of the PMF input, the uncertainty for each species was determined as the sum of 10 % of the VOC concentration and 2 times the method detection limit (MDL) of the species (Paatero, 2000). Tracers for different sources were selected for the model input. For example, CO, ethane and ethyne were the tracers of combustion processes, and methyl chloride (CH_3Cl) was specifically used for biomass burning. DMS (dimethyl sulfide) was a typical tracer for marine emissions, while O_x (i.e., $O_3 + NO_2$) was used as the tracer of secondary formation through photochemical reactions, including the formation of alkyl nitrates, because O_3 shares a common photochemical source with alkyl nitrates (Simpson et al., 2006). In addition to the aforementioned species, alkyl nitrate precursors, including methane, ethane, propane and i/n-butanes, were input into the model. In total, 16 compounds were used for the model input.

Various checks and sensitivity tests were conducted to examine the model performance. Firstly, many different starting seeds were tested and no multiple solutions were found. Secondly, the correlation between the predicted and measured concentration of each species was fairly good at TW ($R^2 = 0.64$–0.94) after the PMF implementation. Thirdly, the scale residuals, which are the uncertainty over the different runs for the input species, ranged between −3 and 3 for the PMF solution. Fourthly, the ratios of Q(robust) / Q(true) were close to 1 for a four-factor solution, within the ranges of 0.97–0.98 at TW and higher than those of three-factor and five-factor solutions, indicating all data points were fit better in the four-factor solution. Indeed, the extracted source profiles from the four-factor solution were the most reasonable. All the factors were mapped to a base factor in all the 100 runs in the bootstrapped simulation for the four-factor solution, suggesting the solution was stable. Lastly, the G-space plot extracted from the F-peak model results did not present oblique edges, reflecting that there was little rotation for the selected solution. Overall, the above features demonstrated that PMF provided reasonable results for the source apportionment of alkyl nitrates (Ling et al., 2011; Ling and Guo, 2014).

2.5 Photochemical box model incorporating Master Chemical Mechanism (PBM–MCM)

A photochemical box model coupled with Master Chemical Mechanism (PBM–MCM) was used to simulate the in situ formation of alkyl nitrates at TMS and TW. The PBM–MCM was developed by assuming that it was a well-mixed box without the treatment of vertical or horizontal dispersion, and the air pollutants in the model were homogeneous. For the mechanism coupled in the model, the MCM (version 3.2) used in this study is a state-of-the-art chemical mechanism, which describes the degradation of 143 primary VOCs including methane and contains around 16 500 reactions involving 5900 chemical species (Jenkin et al., 1997, 2003; Saunders et al., 2003). The measured data, including O_3, CO, NO_x, SO_2, 54 VOCs and methane, together with the actual meteorological conditions of temperature, relative humidity and boundary layer in the region, were used to constrain the model. The photolysis rates of different species in the model were parameterized as suggested by a previous study (Pinho et al., 2009) using the photon flux determined from the Tropospheric Ultraviolet and Visible Radiation (v5) model based on the actual conditions, such as meteorological conditions, location and time period of the field campaign in Hong Kong (Lam et al., 2013). The model output simulated in situ formation of alkyl nitrates and other secondary products as well as the full set of precursors, radicals and intermediates. To provide robust results from the model simulation, several measures were adopted for the model development. The detailed information for the model frameworks, the model development and the evaluation for the model performance has been reported in our previous studies (Lam et al., 2013; Ling et al., 2014).

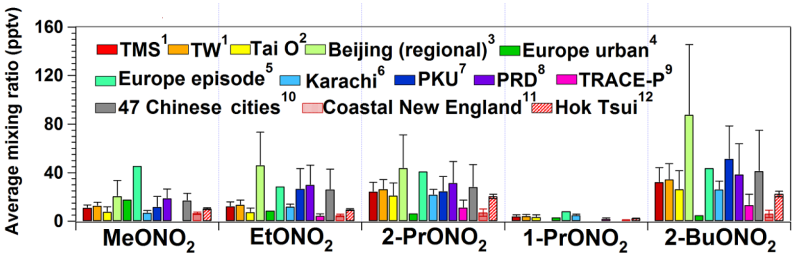

Figure 2. Comparison of alkyl nitrate mixing ratios in different locations. Data collected by UCI before 2008 (PRD and TRACE-P) were adjusted to UCI's new calibration scale to permit direct comparison (see text for details about the new calibration). 1 – this study, September–November 2010. 2 – rural site, August 2001–December 2002 (Simpson et al., 2006). 3 – urban site, 2009–2011 (Wang et al., 2013). 4 – urban sites, April–May 2004 (Worton et al., 2010). 5 – urban sites, April–May 2004 (Worton et al., 2010). 6 – coastal site, December 1998–January 1999 (Barletta et al., 2002). 7 – urban site, August–September 2011 and December 2011–January 2012 (Wang et al., 2013). 8 – regional background sites, September 2009 (Wang et al., 2013). 9 – aircraft measurement, February–April 2001 (Simpson et al., 2003). 10 – urban sites, July 2009 (Wang et al., 2013). 11 – coastal site, January–February and June–August 2002, July–August 2004 (Russo et al., 2010). 12 – regional background site, March 2001–April 2002 (unpublished data).

3 Results and discussion

3.1 Descriptive statistics of alkyl nitrates and their parent hydrocarbons

Table 1 presents the descriptive statistics of alkyl nitrates and their parent hydrocarbons at TMS and TW. Figure 2 compares the levels of alkyl nitrates measured at TMS and TW with those measured in different environments in previous studies. In general, 2-$PrONO_2$ and 2-$BuONO_2$ were the most abundant alkyl nitrates at the two sites, consistent with the results observed in different environments (Blake et al., 2003; Simpson et al., 2006; Russo et al., 2010; Wang et al., 2013). The relatively higher levels of 2-$PrONO_2$ and 2-$BuONO_2$ were associated with the balance between increased branching ratios for photochemical alkyl nitrate formation and the decreased lifetime of both parent alkanes and alkyl nitrates with increasing carbon number (Arey et al., 2001; Simpson et al., 2006; Russo et al., 2010). In comparison, the levels of $MeONO_2$, $EtONO_2$ and 2-$PrONO_2$ were slightly higher at TW than at TMS ($p < 0.05$), with average values of 12.6 ± 0.5 (mean $\pm$ 95 % confidence interval), 13.3 ± 0.6 and 26.3 ± 1.2 pptv, respectively, at TW. The average mixing ratios of 1-$PrONO_2$ and 2-$BuONO_2$ were comparable at the two sites ($p > 0.05$). The results were contradictory to the fact that the mixing ratios of their parent hydrocarbons at TMS were much lower than at TW, highlighting the complexity of sources of alkyl nitrates at both sites.

In comparison with other studies, the average mixing ratios of alkyl nitrates at TMS were much higher than those measured in forested areas in coastal New England (Russo et al., 2010) and in tropospheric air influenced by Asian outflow during the airborne TRACE-P mission (Simpson et al., 2003), where the levels of parent hydrocarbons were also lower. (Note that all of the UCI data shown in Fig. 2 were adjusted to UCI's post-2008 alkyl nitrates' calibration scale to enable direct comparison; Simpson et al., 2011). However, the mean mixing ratios of C_1–C_3 alkyl nitrates were slightly lower and the 2-$BuONO_2$ mixing ratio was higher at TMS than at Tai O (Table 2), Hok Tsui and in Karachi, Pakistan (Barletta et al., 2002; the Karachi data have also been adjusted to the new UCI alkyl nitrates' calibration scale). The differences among TMS, Tai O and Hok Tsui may result not only from the levels of their parent hydrocarbons but also from the influence of air masses with different photochemical ages and sources (Wang et al., 2003). Furthermore, as mentioned in Sect. 2.2, the sampling method and sampling period at TMS were different from those at Tai O and Hok Tsui, where the sampling duration was only 1 min and the sampling time varied on different sampling days. In particular, many whole-air samples were collected during O_3 episodes at Tai O. These could also induce differences in observed levels among the three sites. At the urban TW site, the mean mixing ratios of alkyl nitrates were lower than those measured in urban areas in Europe (Worton et al., 2010) and China (Wang et al., 2013). Compared to the average values of alkyl nitrates at Tai O, the levels of $EtONO_2$, 1-$PrONO_2$ and 2-$BuONO_2$ were slightly higher and the $MeONO_2$ and 2-$PrONO_2$ mixing ratio was lower at TW.

Table S2 and Fig. S2 in the Supplement summarize the synoptic weather conditions and the corresponding variations of O_3 and alkyl nitrates on O_3 episode and non-O_3 episode days at both sites. In general, meteorological conditions including temperatures, winds and solar radiation significantly influenced the levels of air pollutants (Table S2). High mixing ratios of O_3 and alkyl nitrates were usually associated with meteorological conditions with high-pressure system and/or stable conditions, such as high temperatures, intense solar radiation and low wind speeds. Figure 3 shows the time series of C_1–C_4 alkyl nitrates on O_3 episode and non-O_3 episode days at both sites, while Fig. 4 presents the temporal variations of their parent hydrocarbons accordingly. Although the ranges of alkyl nitrate mixing ratios were simi-

Table 1. Descriptive statistics of alkyl nitrates and parent hydrocarbons (pptv) in whole-air samples collected at TMS and TW during the sampling period.

Species	TMS					TW				
	Mean[a]	Min.	Max.	10th[b]	90th[b]	Mean	Min.	Max.	10th[b]	90th[b]
$MeONO_2$	10.9 ± 0.4	6.2	21.4	8.1	13.6	12.6 ± 0.5	7.2	26.6	9.2	16.4
$EtONO_2$	12.1 ± 0.5	3.2	25.6	7.6	16.5	13.3 ± 0.6	4.0	35.0	8.3	18.1
2-$PrONO_2$	24.1 ± 1.1	4.0	51.2	14.8	34.7	26.3 ± 1.2	6.0	49.2	16.2	36.2
1-$PrONO_2$	3.8 ± 0.2	0.4	10.6	1.9	5.5	4.0 ± 0.2	0.7	8.1	2.2	6.1
2-$BuONO_2$	32.0 ± 1.7	3.1	80.1	18.8	46.6	34.2 ± 1.9	5.1	92.8	20.8	49.2
Methane (ppmv)	2.0 ± 0.1	1.8	2.2	1.9	2.0	2.0 ± 0.1	1.8	2.5	1.9	2.0
Ethane	1908 ± 78	396	3588	1154	2470	2224 ± 90	717	4315	1359	2906
Propane	1101 ± 75	106	4455	569	1749	3551 ± 415	1443	33 800	1844	5153
n-Butane	830 ± 91	97	6252	349	1517	4486 ± 482	1372	34 700	2168	7633

[a] Average ±95 % confidence interval. [b] 10th and 90th percentiles.

Table 2. Descriptive statistics of alkyl nitrate (pptv) and parent hydrocarbons (ppbv) in whole-air samples collected at Tai O between 24 August 2001 and 31 December 2002 (from Simpson et al., 2006).

Compound	Minimum	Maximum	Median	Mean
$MeONO_2$	5.5	52.2	13.4	15.9
$EtONO_2$	2.7	34.3	12.1	13.1
1-$PrONO_2$	0.2	14.5	3.5	3.9
2-$PrONO_2$	2.4	65.9	24.5	32.6
2-$BuONO_2$	0.8	89.8	27.4	30.7
Methane (ppmv)	1.75	3.70	1.96	2.05
Ethane (ppbv)	0.38	5.05	2.14	2.12
Propane (ppbv)	0.006	13.0	1.54	2.05
n-Butane (ppbv)	0.006	12.8	0.95	1.64

lar and maximum values were observed in the afternoon, the day-to-day variations of individual alkyl nitrates differed during the sampling period at both sites. The maximum values were comparable and the diurnal patterns tracked each other for the C_3–C_4 alkyl nitrates at TMS and TW, especially on the days (24 October to 3 November, 9 and 19 November) with relatively higher O_3 mixing ratios ($p < 0.05$). The average daytime O_3 mixing ratios (07:00–18:00) on the high-O_3 days were 77 ± 3 and 38 ± 3 ppbv at TMS and TW, respectively, compared to 58 ± 3 and 23 ± 3 ppbv on the non-O_3 episode days. Typically, the average daytime levels of 2-$PrONO_2$, 1-$PrONO_2$ and 2-$BuONO_2$ on high-O_3 days at TMS were 27 ± 1 (TW: 28 ± 1), 4.5 ± 0.3 (4.4 ± 0.2) and 37 ± 2 (39 ± 3) pptv, respectively, higher than those on non-O_3 episode days ($p < 0.05$), implying that secondary formation of alkyl nitrates may be more prominent on O_3 episode days. Coincident with the high C_3–C_4 alkyl nitrates during high-O_3 days, their parent hydrocarbons, i.e., propane (0.56–4.46 and 1.55–10.4 ppbv for TMS and TW, respectively) and *n*-butane (0.28–6.25 and 1.47–16.1 ppbv, respectively) also showed elevated mixing ratios (Fig. 4), further suggesting an important source of C_3–C_4 alkyl nitrates, which was photooxidation of the parent hydrocarbons. For the C_1–C_2 alkyl nitrates, the temporal patterns of $MeONO_2$ and $EtONO_2$ were different at the two sites, especially on high-level O_3 days. The peaks of $MeONO_2$ and $EtONO_2$ were usually observed between 11:00 and 16:00 LT at TMS, except for 14 and 28 October and 1–2, 9 and 20–21 November. The peaks of C_1–C_2 alkyl nitrates corresponded to the high levels of methane and ethane observed at 11:00 to 17:00 LT, likely resulted from regional transport (Guo et al., 2009; Jiang et al., 2010) and/or mesoscale circulation (Gao et al., 2005; Wang et al., 2006) (Sect. 3.2.3). At TW, however, besides the maximum concentrations observed in the afternoon, high levels of $MeONO_2$ and $EtONO_2$ were observed from midnight to early morning on 13 out of the 19 sampling days (i.e., 2, 8, 14, 24, 28 and 30–31 October and 1–3 and 19–21 November), when the prevailing winds switched to the southeast direction, implying that the high levels of $MeONO_2$ and $EtONO_2$ are likely related to marine emissions and aged continental plumes which were recirculated from the South China Sea to the coastal urban site at night. Indeed, this speculation was supported by the source apportionment results at TW, which confirmed that the high $MeONO_2$ and $EtONO_2$ levels from midnight to early morning on the above sampling days were related to oceanic emissions (see Sect. 3.2.2 for details).

Although the levels of the parent hydrocarbons were lower at TMS, similar values of alkyl nitrates were observed at both sites, regardless of the elevation, suggesting the contributions of different sources and/or the influences of different air masses. Hence, the source apportionments of alkyl nitrates, contributions of reaction pathways for the secondary formation of alkyl nitrates, and the relationship between O_3 and alkyl nitrates are analyzed in the following sections.

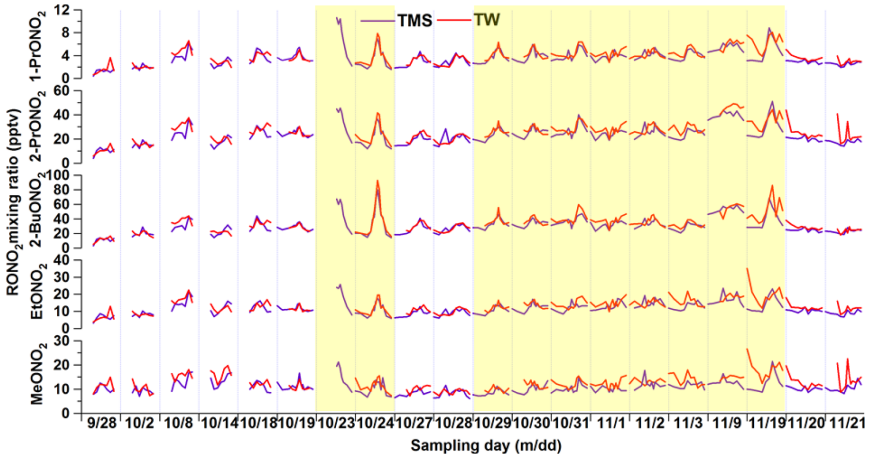

Figure 3. Time series of $MeONO_2$, $EtONO_2$, 1-$PrONO_2$, 2-$PrONO_2$ and 2-$BuONO_2$ measured at TMS (purple) and TW (red) in 2010. The yellow shading highlights the O_3 episode days.

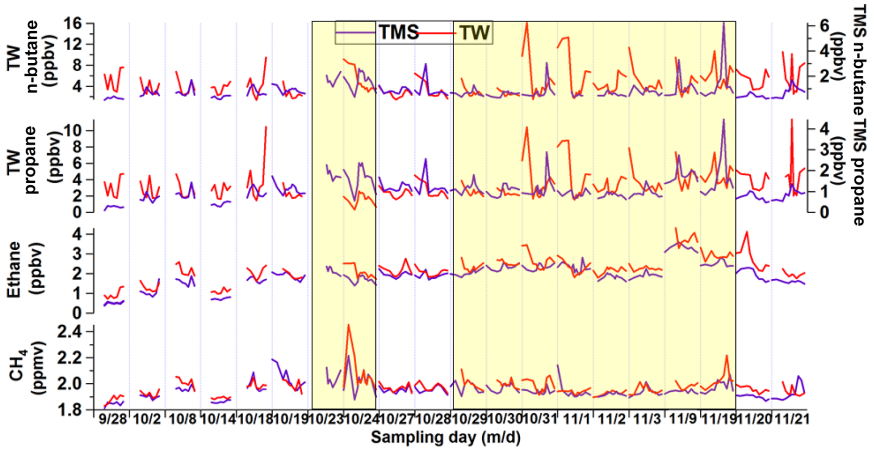

Figure 4. Time series of the parent hydrocarbons of alkyl nitrates at TMS and TW. The yellow shading highlights the O_3 episode days.

3.2 Sources of alkyl nitrates

3.2.1 Photochemical evolution of alkyl nitrates

As photochemical oxidation of parent hydrocarbons is an important source of alkyl nitrates, it is valuable to study the photochemical evolution of alkyl nitrates. To do so, the relationships of alkyl nitrates with their parent hydrocarbons at the two sites were further examined using a simplified sequential reaction model developed by Bertman et al. (1995) (Eq. 1), based on the assumptions that (i) the hydrogen abstraction reaction from the parent hydrocarbon was the rate-limiting step for photochemical production of alkyl nitrates and (ii) the reaction environment was NO_x-rich, making the reaction with NO the dominant pathway for the removal of RO_2 radicals (Russo et al., 2010). In this study, the average mixing ratios of NO_x at TMS and TW were 10.7 ± 0.3 and 56.3 ± 1.6 ppbv, respectively, indicating that the environment was NO_x-rich (> 0.1 ppbv, Roberts et al., 1998). Hence, reaction with NO was the main pathway for the removal of RO_2 radicals at the two sites. In addition, the results of the PBM–MCM model simulation confirmed that the hydrogen abstraction reaction from the parent hydrocarbon, namely the reaction of hydrocarbon with OH radical, was indeed the rate-limiting step for photochemical production of alkyl nitrates at both sites (Lyu et al., 2015).

$$\frac{\mathrm{RONO_2}}{\mathrm{RH}} = \frac{\beta k_\mathrm{A}}{k_\mathrm{B} - k_\mathrm{A}} \left(1 - e^{(k_\mathrm{A} - k_\mathrm{B})t}\right) + \frac{[\mathrm{RONO_2}]_0}{[\mathrm{RH}]_0} e^{(k_\mathrm{A} - k_\mathrm{B})t}, \quad (1)$$

where $\beta = \alpha_1 \alpha_2$ and k_A is the production rate for the formation of alkyl nitrates through the oxidation of hydrocarbons, RH ($k_\mathrm{A} = k_1[\mathrm{OH}]$), while k_B is the destruction rate for alkyl nitrates through photolysis and the reaction with OH ($k_\mathrm{B} = k_5[\mathrm{OH}] + J_{\mathrm{RONO_2}}$). $[\mathrm{RONO_2}]_0$ and $[\mathrm{RH}]_0$ are the initial concentrations of alkyl nitrates and the parent hydrocar-

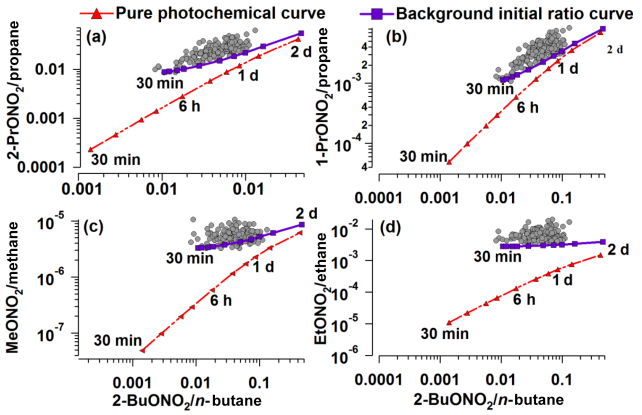

Figure 5. Relationships of C_1–C_3 $RONO_2$ / RH with 2-$BuONO_2$ / *n*-butane at TMS. The red dashed curves were obtained based on zero initial concentrations of RH and alkyl nitrates (pure photochemical curves, PP), while the blue solid curves were obtained based on non-zero initial levels (background initial ratio curves, BIR), with the lowest ratios of $RONO_2$ / RH from 00:00 to 07:00 LT.

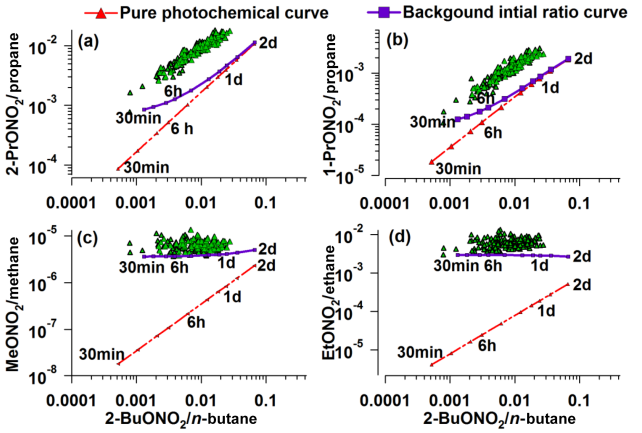

Figure 6. Relationships of C_1–C_3 $RONO_2$ / RH with 2-$BuONO_2$ / *n*-butane at TW. The red dashed curves were obtained based on zero initial concentrations of RH and alkyl nitrates (pure photochemical curves, PP), while the blue solid curves were obtained based on non-zero initial levels (background initial ratio curves, BIR), with the lowest ratios of $RONO_2$ / RH from 00:00 to 07:00 LT.

bons before photochemical processing, respectively; [OH] is the diurnal average concentration of the OH radical. The relationships of alkyl nitrates with their parent hydrocarbons derived from the preceding equation are comparatively independent of the variations of OH and photolysis rates of alkyl nitrates (Roberts et al., 1998; Wang et al., 2013). If the initial concentrations of alkyl nitrates and RH are zero, Eq. (1) can be expressed as follows (Eq. 2):

$$\frac{\mathrm{RONO_2}}{\mathrm{RH}} = \frac{\beta k_\mathrm{A}}{k_\mathrm{B} - k_\mathrm{A}}(1 - e^{(k_\mathrm{A} - k_\mathrm{B})t}). \quad (2)$$

The relationships between alkyl nitrates and RH are obtained by plotting the measured ratios of $RONO_2$ / RH to a specific ratio, 2-$BuONO_2$ / *n*-butane. The 2-$BuONO_2$ / *n*-butane ratio has been widely used in the analysis of alkyl nitrates because *n*-butane is typically one of the most abundant hydrocarbons and 2-$BuONO_2$ is the dominant alkyl nitrate (Roberts et al., 1998; Wang et al., 2013; Worton et al., 2010). Although some studies have investigated the relationships between alkyl nitrates and their parent hydrocarbons using zero initial values of alkyl nitrates, more recent studies have used non-zero initial values of alkyl nitrates to evaluate the influence of background levels on the photochemical evolution of alkyl nitrates (Reeves et al., 2007; Russo et al., 2010; Wang et al., 2013). Therefore, in addition to zero initial ratios, non-zero initial ratios of $RONO_2$ / RH, equal to the lowest values from 00:00 to 07:00 measured at TMS and TW, respectively, as suggested by Wang et al. (2013), were used to investigate the relationships between alkyl nitrates and their parent hydrocarbons in this study. The diurnal average OH mixing ratios were simulated using the PBM–MCM (Lyu et al., 2016). By providing the values of photochemical processing time (t), the predicted ratios of $RONO_2$ / RH were calculated since other parameters, i.e., k_A, k_B, α_1, α_2 and $J_{\mathrm{RONO_2}}$, were obtained from literature (Clemitshaw et al., 1997; Simpson et al., 2003; Worton et al., 2010; Wang et al., 2013). In this study, the given photochemical processing time ranged from 30 min to 2 days. The curves generated with zero initial values were the pure photochemical (PP) curves for the evolution of alkyl nitrates, and the curves with non-zero values, defined as background initial ratio (BIR) curves, were generated by assuming that both photochemical formation and background levels contributed to the distribution of alkyl nitrates (Russo et al., 2010; Wang et al., 2013). Consistent with previous studies (Russo et al., 2010; Wang et al., 2013), the shapes of the BIR curves were different from those of PP curves. The BIR curves of C_1–C_3 alkyl nitrates at both sites were positioned above their PP curves at a shorter processing time ($t < 1$ day) and converged towards the PP curves at longer processing times ($t = 1.5$–2 day) (Fig. 5), resulting from the decreased influence of the parameter $\frac{[\mathrm{RONO_2}]_0}{[\mathrm{RH}]_0} e^{(k_\mathrm{A} - k_\mathrm{B})t}$ on the difference between the two curves as the photochemical age increased (Wang et al., 2013). This feature was more pronounced for C_3–C_4 alkyl nitrates at TW (Fig. 6) because of the lower values of $[RONO_2]_0$ / $[RH]_0$ resulting from the high mixing ratios of propane and *n*-butane (Ling and Guo, 2014). Figure 5 presents the relationships of C_1–C_3 $RONO_2$ / RH to 2-$BuONO_2$ / *n*-butane at TMS. The red dashed curves are pure photochemical curves, while the blue solid curves are BIR curves with the lowest ratios of $RONO_2$ / RH from 00:00 to 07:00 LT as the background initial ratio. Similarly, Fig. 6 shows the relationships of C_1–C_3 $RONO_2$ / RH to 2-$BuONO_2$ / *n*-butane at TW.

At TMS, the measured ratios of $MeONO_2$ / methane and $EtONO_2$ / ethane to 2-$BuONO_2$ / *n*-butane were much higher than the ratios in the PP curves (Fig. 5c, d), with the observed ratios larger than their theoretical ratios by factors of 5–25. As expected, the observed trends approached the PP curves at a longer processing time, suggesting that the measured ratios of C_1–C_2 $RONO_2$ / RH to 2-$BuONO_2$ / *n*-butane were influenced by aged air masses resulting from their relatively long atmospheric lifetimes and the slow photochemical reaction rates of methane and ethane (Worton et al., 2010; Russo et al., 2010). However, the difference between the measured ratios and the predicted ratios of C_1–C_2 $RONO_2$ / RH to 2-$BuONO_2$ / *n*-butane in BIR curves was comparatively smaller, further confirming that there were other sources contributing to ambient C_1–C_2 alkyl nitrates besides photochemical formation, including the background levels of C_1–C_2 alkyl nitrates and their parent hydrocarbons (direct measurements of RH in Table 1) (Wang et al., 2013). For example, the average $MeONO_2$ and $EtONO_2$ mixing ratios at Hok Tsui, a PRD regional background site, were 10.4 ± 0.7 and 9.6 ± 0.7 pptv (unpublished data, 2001–2002), respectively.

Regarding the C_3 alkyl nitrates, the measured ratios of 1- and 2-$PrONO_2$ / propane to 2-$BuONO_2$ / *n*-butane were closer to the ratios of the BIR curve than those of the PP curve at TMS, further indicating the influence of background C_3 alkyl nitrates and their parent hydrocarbons. However, the evolution of the measured ratios of C_3 $RONO_2$ / RH to 2-$BuON_2$ / *n*-butane agreed well with the predicted ratios of BIR and PP curves at TMS, indicating that secondary formation from propane oxidation contributed significantly to the ambient C_3 alkyl nitrates, including the background C_3 alkyl nitrates. Consistent with previous studies, the slopes of the observed ratios of C_3 $RONO_2$ / RH to 2-$BuONO_2$ / *n*-butane were different from those in the PP and BIR curves (Russo et al., 2010; Wang et al., 2013). For example, the slopes of the observed ratios of 1- and 2-$PrONO_2$ / propane to 2-$BuONO_2$ / *n*-butane were 0.04 ± 0.01 and 0.26 ± 0.02, respectively, while the slopes for the BIR curves were 0.02 ± 0.01 (PP curve: 0.02 ± 0.01) and 0.12 ± 0.01 (0.10 ± 0.01), respectively. This was reasonable as the difference in the number of samples and distribution of data between the observed ratios and the ratios of PP and BIR curves, particularly when the observed ratios were higher than the theoretical ones because of significant influence of the background levels of alkyl nitrates and RH (Russo et al., 2010; Wang et al., 2013). Therefore, to further investigate the influence of secondary formation and background mixing ratios on C_3 alkyl nitrates at TMS, the ratio of 1- / 2-$PrONO_2$ was examined. Previous studies reported that the theoretical ratio of 1- / 2-$PrONO_2$ was the ratio between the yield for 1-$PrONO_2$ and 2-$PrONO_2$ formation, which was equal to the ratio of $\beta_{1\text{-PrONO2}} / \beta_{2\text{-PrONO2}}$ (0.21) (Simpson et al., 2003; Wang et al., 2013). If photochemical production was the dominant source of 1-$PrONO_2$ and 2-$PrONO_2$, the observed ratios should be close to the theoretical ones. Indeed, the slope of 1-$PrONO_2$ and 2-$PrONO_2$ at TMS was 0.19 ($R^2 = 0.86$, $p < 0.05$), close to the theoretical ratio (0.21), confirming that photochemical production from propane, including in situ photochemical production and transport of photochemically formed C_3 alkyl nitrates in urban areas and/or during transit from urban areas to TMS, was the dominant source of ambient C_3 alkyl nitrates.

At TW, the comparison between the observed ratios of C_1–C_2 $RONO_2$ / RH to 2-$BuONO_2$ / *n*-butane and the ratios from the PP and BIR curves was consistent with that at TMS. However, in terms of C_3 alkyl nitrates, although the evolution of the measured ratios of C_3 $RONO_2$ / RH to 2-$BuONO_2$ / *n*-butane followed the trends of the ratios in the PP and BIR curves, the measured ratios of C_3 $RONO_2$ / RH to 2-$BuONO_2$ / *n*-butane at TW were further away from the PP/BIR curves and about 2–3 times the ratios in the PP and BIR curves, implying additional sources of C_3 alkyl nitrates (Wang et al., 2013) (details in Sect. 3.2.2). High emissions of propane provided sufficient precursors of C_3 alkyl nitrates, and the lifetimes of 1-$PrONO_2$ and 2-$PrONO_2$ were long enough to sustain relatively high levels at TW. To further investigate the influence of additional sources on the distributions of C_3 alkyl nitrates at TW, Eq. (1) was used to fit the measured ratios of 1- and 2-$PrONO_2$ / propane to calculate the yield of C_3 alkyl nitrates (β). The average yields of 1- and 2-$PrONO_2$ were 0.032 ± 0.004 and 0.22 ± 0.02, respectively, higher than the laboratory kinetic values by factors of 4–9 (Kwok and Atkinson, 1995). This confirms the presence of additional emissions of C_3 alkyl nitrates at TW, including locally emitted C_3 alkyl nitrates and/or secondary formation other than the production pathway from propane to peroxyl radical and $PrONO_2$ (Reeves et al., 2007; Worton et al., 2010). The slope of 1-$PrONO_2$ to 2-$PrONO_2$ at TW was 0.15 ($R^2 = 0.80$, $p < 0.05$), lower than the theoretical ratio of 0.21, further demonstrating the influence of other significant sources on ambient mixing ratios of C_3 alkyl nitrates at TW.

3.2.2 Source apportionment of alkyl nitrates

Figure 7 presents the explained variations of species (as a percentage of the species total) in the identified sources extracted by the PMF model. The standard error in Fig. 7 was obtained from a bootstrap analysis of the PMF model simulation. The source profiles of the alkyl nitrates and their parent hydrocarbons were altered resulting from photochemical transformation during transport to the TMS site. Therefore, only the data collected at the urban site were used for source apportionments of alkyl nitrates.

High concentrations of O_x and alkyl nitrates were found in the first factor at both sites, implying that this factor was associated with secondary formation. In addition, certain amounts of combustion species, such as ethane, ethyne, propane, *i*/*n*-butanes, benzene and CO, were present in this factor. It is not surprising that O_x correlated with the afore-

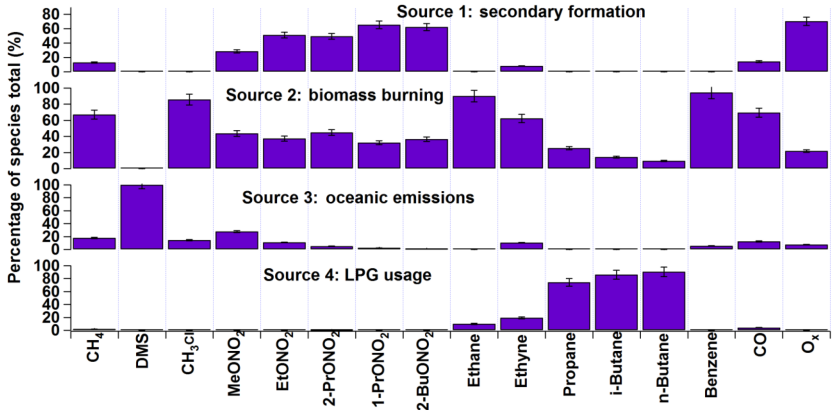

Figure 7. Explained variations of species in the identified sources extracted by the PMF model for TW.

mentioned species given that O_3 is a secondary pollutant formed from photochemical oxidation of RH (Ling and Guo, 2014). The second factor was distinguished by a significant presence of methyl chloride, ethene, ethyne and benzene along with certain amounts of methane, propane and i/n-butane. It is well established that methyl chloride, ethyne and benzene are typical tracers for biomass burning and biofuel combustion (Barletta et al., 2009; Guo et al., 2011). As biofuel was not in widespread use in Hong Kong (HKCSD, 2010), this factor was identified as biomass burning. The third factor was identified as oceanic emissions, as the tracer DMS had an exclusively high percentage in this source at both sites (Blake et al., 2003; Marandino et al., 2013). The last factor was dominated by high percentages of propane and i/n-butanes, typical tracers of liquefied petroleum gas (LPG). Therefore, this factor was identified as LPG usage.

As mentioned earlier, regional transport and mesoscale circulation had a significant influence on the distribution of air pollutants at TMS and TW (Guo et al., 2012, 2013a). By using the Weather Research and Forecasting (WRF) model, air masses affected by mesoscale circulation were distinguished from those affected by regional transport (Guo et al., 2013a). Nine sampling days during the entire sampling period (24 and 29–31 October, 1–3, 9 and 19 November) were identified as affected by mountain-valley breezes (they were also O_3 episode days). Hence, we divided the sampling period into two categories: "meso" and "non-meso" scenarios for source apportionment analysis. The meso scenario included the 9 O_3 episode days with apparent mesoscale circulation, while the non-meso scenario covered the rest of the sampling days.

By summing up the mass of the alkyl nitrates in each source category, the overall mixing ratios in each source were obtained and the contribution of each individual source to alkyl nitrates at both sites was calculated. Figures 8 and 9 present the source contributions to individual alkyl nitrates for the meso and non-meso scenarios in percentage and in mixing ratio at TW, respectively. The mixing ratios of total alkyl nitrates (i.e., $\sum RONO_2 = MeONO_2 + EtONO_2 + 1\text{-}PrONO_2 + 2\text{-}PrONO_2 + 2\text{-}BuONO_2$) were higher in the meso scenario than those in non-meso scenario ($p < 0.05$), with the average value of 100.9 ± 7.5 pptv for total alkyl nitrates in the meso scenario about 1.4 times that in the non-meso scenario. It was found that in the meso scenario, secondary formation was the most significant contributor to the total alkyl nitrate mixing ratios, with an average percentage of 60 ± 2 % or absolute mixing ratio of 60.2 ± 1.2 pptv, followed by biomass burning (34 ± 1 % or 35.1 ± 0.4 pptv) and oceanic emissions (6 ± 1 % or 5.62 ± 0.06 pptv). For the non-meso scenario, the contributions of biomass burning (46 ± 2 % or 34.2 ± 0.7 pptv) and secondary formation (44 ± 2 % or 32.9 ± 0.7 pptv) were comparable, and the oceanic emissions contributed 10 ± 1 % or 7.0 ± 0.07 pptv to the total alkyl nitrates. The higher contribution of secondary formation in the meso scenario at TW was mainly associated with a higher degree of photochemical reactions. Indeed, the PBM–MCM model simulation indicated that the average concentration of HO_x ($HO_x = OH + HO_2$) during daytime hours (07:00–18:00 LT) in the meso scenario was $(2.5 \pm 0.7) \times 10^7$ molecule cm^{-3}, about twice that of the non-meso scenario.

In addition, although the percentage contribution of biomass burning was higher in the non-meso scenario, the absolute mixing ratios of biomass burning were comparable in the two scenarios. Figure 10 shows the diurnal patterns of $\sum RONO_2$ from biomass burning and oceanic emissions in meso and non-meso scenarios at TW. The contribution of biomass burning in the meso scenario was likely attributable to local emissions, including the cooking and heating activities in the small villages nearby and the frequent barbecue activities at the base of the mountain (Guo et al., 2013a, b), as well as the forest fires observed in the mountainous areas (AFCD, 2015). The regular cooking and heating activities from 07:00 to 14:00 LT in many dim sum restaurants in the village likely resulted in the increased levels of biomass burning in the morning until noon. In contrast, the diurnal

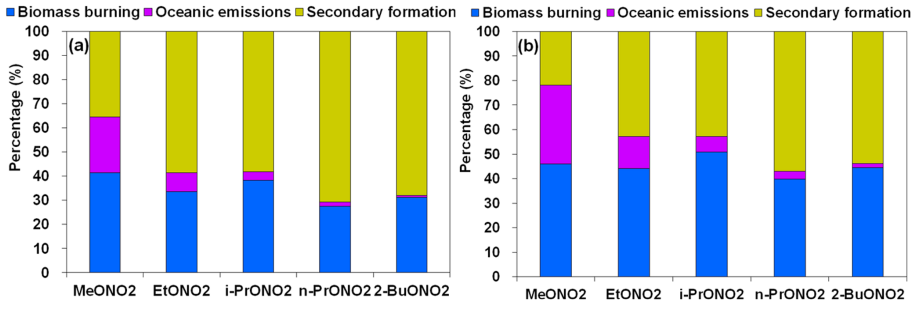

Figure 8. Source contributions to individual alkyl nitrates in **(a)** meso and **(b)** non-meso scenarios at TW (in percentage).

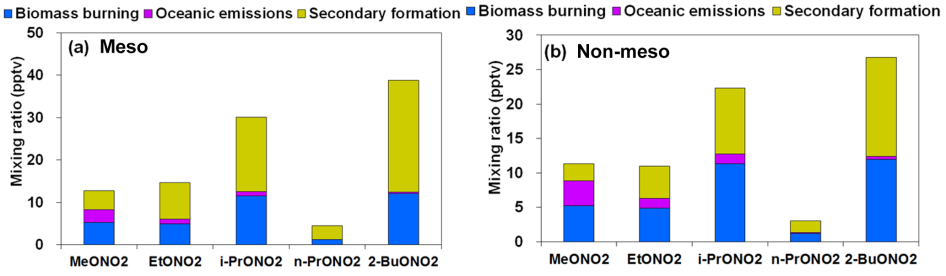

Figure 9. Source contributions to individual alkyl nitrates in **(a)** meso and **(b)** non-meso scenarios at TW (in summed mixing ratio).

pattern in the non-meso scenario was weak and the maximum values were not statistically different from the minimum values. The difference of the average mixing ratio of $\sum RONO_2$ between daytime and nighttime hours was only 1 pptv for biomass burning. The weak diurnal variations in the non-meso scenario suggests that the contribution of fresh biomass burning emissions was insignificant, revealing the influence of regional transport from the PRD region. This speculation was confirmed by the analysis of 12 h backward trajectories, which showed that air masses in the non-meso scenario were mainly from the inland PRD region (not shown). It is noteworthy that although air masses were more aged in the non-meso scenario, the levels of alkyl nitrates were comparable to those in the meso scenario, highlighting the strong emissions of biomass burning in the PRD region (Yuan et al., 2010).

For the oceanic emissions, a minimum mixing ratio during daytime hours was found for $\sum RONO_2$ in the meso scenario, while a broad peak was present during daytime hours in the non-meso scenario. The daytime minimum mixing ratio in the meso scenario at TW was related to uplifted valley breezes that brought alkyl nitrates away from TW to TMS, while the higher nighttime values were probably owing to marine emissions and aged continental plumes which were recirculated from the South China Sea to the coastal urban site at night. In contrast, the broad daytime peak in the non-meso scenario was likely associated with higher daytime temperature and solar radiation, leading to higher oceanic emissions that were transported from eastern China and southern China coastal regions to the TW site.

Moreover, the contributions of oceanic emissions to C_1–C_2 alkyl nitrates were higher than C_3–C_4 alkyl nitrates, with average percentages of 23 and 32 % for the meso and non-meso scenarios (Figs. 8 and 9), suggesting the importance of oceanic emissions to C_1–C_2 alkyl nitrates, consistent with the results of previous work (Simpson et al., 2003). The C_3–C_4 alkyl nitrates were dominated by the secondary formation in the meso scenario (58–71 %), while the contributions of biomass burning and secondary formation to C_3–C_4 alkyl nitrates were comparable in the non-meso scenario.

3.2.3 Contributions of mesoscale circulation, in situ formation and regional transport to alkyl nitrates at TMS

Valley breezes transported freshly emitted parent hydrocarbons and alkyl nitrates from the urban areas at the base of the mountain (TW) to the mountain summit (TMS) during daytime hours, redistributing the ambient levels of alkyl nitrates at TMS (Guo et al., 2013a; Lam et al., 2013). Except for $MeONO_2$, which had comparable levels in both meso and non-meso scenarios, the mixing ratios of daytime C_2–C_4 alkyl nitrates were all higher in meso scenario than those in non-meso scenario ($p < 0.05$), with average values of 14.21 ± 0.79, 28.73 ± 1.70, 4.67 ± 0.29 and 40.21 ± 2.79 pptv for $EtONO_2$, i-$PrONO_2$, n-$PrONO_2$ and 2-$BuONO_2$, respectively. To quantify the influence of mesoscale circulation on the mixing ratios of alkyl nitrates at TMS, a moving box model coupled with the Master Chemical Mechanism (Mbox) was applied to the data collected on

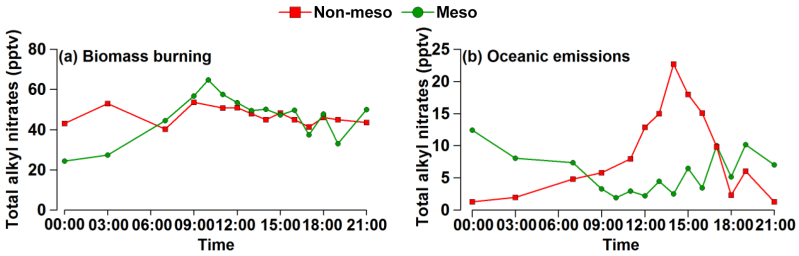

Figure 10. Diurnal patterns of **(a)** biomass burning and **(b)** oceanic emissions for meso and non-meso scenarios at TW.

the days influenced by mesoscale circulation (i.e, the meso scenario) (Guo et al., 2013a). The model was developed based on an idealized trajectory movement between TMS and TW sites, with air pollutants transported from TW to TMS through the valley breeze during daytime hours (08:00–17:00 LT) when the photochemical formation of alkyl nitrates was occurring, contributing to their ambient levels at TMS. As such, the model was only constrained with the observed daytime data at TW. On the other hand, the nighttime downslope flow occurred because of the mountain breeze after sunset until the next morning, and TMS was set as the center of the box model, which was constrained by the data collected at TMS only for that period (Lam et al., 2013).

Table 3 presents the average concentrations of C_1–C_4 alkyl nitrates simulated by the Mbox model at TMS, i.e., the values under the meso scenario. It should be noted that the comparison was only made for daytime alkyl nitrates (08:00–17:00 LT), when the valley breeze occurred. The average mixing ratios of $MeONO_2$, $EtONO_2$, 1-$PrONO_2$, 2-$PrONO_2$ and 2-$ButONO_2$ at daytime hours estimated using the Mbox model were 9.97 ± 0.85, 7.38 ± 0.44, 3.08 ± 0.16, 18.7 ± 0.77 and 34.7 ± 3.14 pptv, respectively, accounting for 86, 52, 66, 65 and 86 % of the observed values at TMS during the same period, respectively. These results demonstrate that when there was mesoscale circulation, the alkyl nitrate levels at TMS were dominated by the photooxidation of their parent hydrocarbons that originated from the urban site TW. Although the mixing ratios of the parent hydrocarbons were lower at TMS, this is still one possible explanation leading to the similar levels of alkyl nitrates measured at the two sites.

For the non-meso scenario, the simulated levels of in situ formation of $MeONO_2$, $EtONO_2$, 1-$PrONO_2$, 2-$PrONO_2$ and 2-$ButONO_2$ at TMS were 3.61 ± 0.48, 2.18 ± 0.29, 1.03 ± 0.13, 3.68 ± 0.45 and 10.9 ± 1.31 pptv, respectively, accounting for 18–42 % of the observed C_1–C_4 alkyl nitrates, indicating that other sources rather than local photochemical formation made significant contributions to ambient levels of alkyl nitrates. As stated earlier, TMS was a mountain site with sparse anthropogenic emissions nearby. However, the prevailing synoptic northerly winds in the non-meso scenario suggested possible regional sources of alkyl nitrates from the inland PRD region to the mountain site. The impact of regional transport on the variations of air pollutants at TMS for the days without mesoscale circulation, especially when the prevailing winds were from the north and had high speeds, was corroborated in Guo et al. (2013a). By excluding the locally formed alkyl nitrates from their overall levels, the contribution of regional sources to alkyl nitrates was determined for TMS. The regional source contributions to $MeONO_2$, $EtONO_2$, 1-$PrONO_2$, 2-$PrONO_2$ and 2-$BuONO_2$ were 7.07 ± 0.50, 8.44 ± 0.62, 2.11 ± 0.22, 16.86 ± 1.17 and 15.15 ± 1.49 pptv, respectively, accounting for 58–82 % of the alkyl nitrates measured at TMS. It is noteworthy that the regional alkyl nitrates included influences from all source categories (photochemical formation, biomass burning and oceanic emissions) for the inland PRD region.

3.3 Relationship of alkyl nitrates with O_3

Alkyl nitrates are mainly formed through the reaction of peroxy radical (RO_2) and NO. However, NO can be oxidized by RO_2 to form NO_2, which results in tropospheric O_3 formation through NO_2 photolysis. Hence, investigating the relationship between alkyl nitrates and O_3 is useful for evaluating the influence of alkyl nitrates on O_3 formation (Simpson et al., 2006). Since the photochemical formation of O_3 and alkyl nitrates occurs during daytime hours, the relationship between O_3 and alkyl nitrates is usually evaluated using the observed daytime data (i.e., 09:00–16:00 LT). In this study, the "oxidant" O_x ($O_3 + NO_2$) was considered to be a better representation of O_3 levels as it takes into account the effect of O_3 titration by NO. Figure 11 shows the correlation between O_x and the total alkyl nitrates ($\sum RONO_2$) at daytime hours. Good correlations were found at TMS ($R^2 = 0.63$) and TW ($R^2 = 0.56$) with the slopes of 0.67 and 0.47 ppbv $pptv^{-1}$, respectively, suggesting that when 1 pptv of total alkyl nitrates was formed from the reaction of RO_2 and NO, 0.67 and 0.47 ppbv of O_x could be simultaneously produced at TMS and TW, respectively. The relatively higher slope at TMS than at TW was owing to higher concentrations of HO_x radicals and higher photochemical reactivity of VOCs at TMS (Lyu et al., 2016). Additionally, as the formation of alkyl nitrates consumes NO, this process results in a negative contribution to O_3 formation. To quantify the negative influence on O_3, the PBM–MCM model was

Table 3. Mixing ratios of C_1–C_4 alkyl nitrates influenced by mesoscale circulation (meso), in situ formation and regional transport at TMS (unit: pptv).

Scenario	$MeONO_2$	$EtONO_2$	1-$PrONO_2$	2-$PrONO_2$	2-$BuONO_2$
Meso	9.97 ± 0.85	7.38 ± 0.44	3.08 ± 0.16	18.7 ± 0.77	34.7 ± 3.14
In situ formation	3.61 ± 0.48	2.18 ± 0.29	1.03 ± 0.13	3.68 ± 0.45	10.9 ± 1.31
Regional transport	7.07 ± 0.50	8.44 ± 0.62	2.11 ± 0.22	16.86 ± 1.17	15.15 ± 1.49

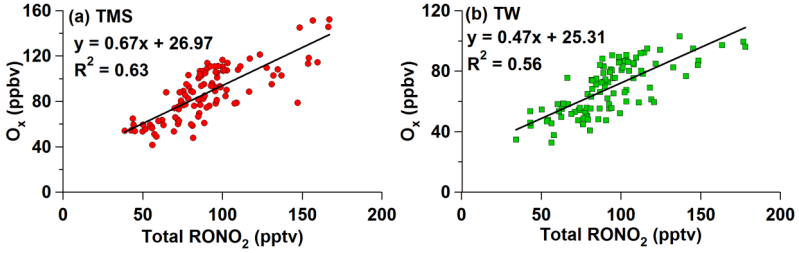

Figure 11. Correlation between O_x ($O_3 + NO_2$) and total alkyl nitrates at **(a)** TMS and **(b)** TW.

applied to the whole data collected at TMS and TW (Lyu et al., 2016). The formation of alkyl nitrates made negative contributions to the O_3 production, with an average reduction of 64.6 (TW: 24.9), 37.4 (11.0), 18.9 (2.6), 39.6 (11.1) and 115.1 (40.6) pptv of O_3 for the formation of $MeONO_2$, $EtONO_2$, 1-$PrONO_2$, 2-$PrONO_2$ and 2-$BuONO_2$ at TMS, respectively. Furthermore, moderate to good correlation was found between the simulated O_3 reduction and the photochemically formed alkyl nitrates at TMS ($R^2 = 0.42$) and TW ($R^2 = 0.72$), with an average O_3 reduction rate of 4.1 and 4.7 pptv pptv^{-1}, respectively. O_3 was reduced by 4.1 and 4.7 pptv if 1 pptv of alkyl nitrates was formed at TMS and TW, respectively.

Moreover, because secondary alkyl nitrates are formed through two main reaction pathways, "$RO_2 + NO$" and "$RO + NO_2$", it is of interest to investigate the relative contribution of the above pathways to the formation of alkyl nitrates. Two scenarios for model simulations were run and compared. The first scenario was the base case in which the model was run with all reaction pathways opened, while the second scenario was the constrained case in which the pathway of $RO_2 + NO \rightarrow RONO_2$ was shut down. It was found that the reaction of $RO_2 + NO$ was the prominent pathway for the secondary formation of alkyl nitrates at the two sites. The contributions of $CH_3O_2 + NO$ to $MeONO_2$ accounted for about 72 and 50 % of the secondarily formed $MeONO_2$, while the contributions of $RO_2 + NO$ were 97–99 and 95–99 % of the secondarily formed C_2–C_4 alkyl nitrates at TMS and TW, respectively. These results are similar to the findings obtained at Tai O, Hong Kong (Lyu et al., 2015). The lower contributions of $RO_2 + NO$ to $MeONO_2$ at the two sites were related to the higher levels of CH_3O from the oxidation of CH_4 and the decomposition of larger RO_2 radicals.

4 Conclusions

Intensive field measurements of alkyl nitrates and their parent hydrocarbons were conducted concurrently at a mountain site (TMS) and an urban site (TW) at the base of the same mountain in Hong Kong from September to November 2010. The levels of $MeONO_2$, $EtONO_2$ and 2-$PrONO_2$ were slightly higher at TW than at TMS ($p < 0.05$), while the average mixing ratios of 1-$PrONO_2$ and 2-$BuONO_2$ were comparable at the two sites ($p > 0.05$). However, the levels of the parent hydrocarbons of alkyl nitrates were lower at TMS, implying the complexity of sources of alkyl nitrates. Receptor model and photochemical box model simulations found that mesoscale circulation and regional transport had a significant impact on the levels of alkyl nitrates at the two sites. At TW, secondary formation was the dominant contributor to alkyl nitrates when there was mesoscale circulation, while the contributions of secondary formation and biomass burning were comparable under the influence of regional transport. At TMS, photooxidation of the parent hydrocarbons from TW contributed 52–85 % to the ambient levels of alkyl nitrates on the days with mesoscale circulation between the two sites. On the other hand, alkyl nitrates from the inland PRD region were responsible for 58–82 % of the observed values at TMS on the days with regional influence. The photooxidation of parent hydrocarbons from TW and regional transport resulted in similar values of alkyl nitrates observed at the two sites. With regard to the secondarily formed alkyl nitrates, the reaction of RO_2 and NO was the prominent pathway at both sites. Moreover, the formation of alkyl nitrates made negative contributions to the O_3 formation, with a reduction rate of 4.1 and 4.7 pptv O_3 per pptv alkyl nitrates at TMS and TW, respectively. The findings of this study will aid in understanding the source contributions and photochemical

formation pathways of alkyl nitrates in Hong Kong's mountainous areas.

5 Data availability

The data set is available to the community and can be accessed by request to Hai Guo (ceguohai@polyu.edu.hk) of the Hong Kong Polytechnic University.

The Supplement related to this article is available online at doi:10.5194/acp-16-8141-2016-supplement.

Acknowledgements. This project was supported by the Research Grants Council of the Hong Kong Special Administrative Region via grants PolyU5154/13E, PolyU152052/14E and CRF/C5022-14G. This study was partly supported by the internal grants of the Hong Kong Polytechnic University (4-BCAV and 1-ZVCX) and the National Natural Science Foundation of China (No. 41405112 and 41275122). The challenging but ultimately very helpful comments of the anonymous reviewers are greatly appreciated.

Edited by: S. Brown
Reviewed by: two anonymous referees

References

AFCD (Agriculture, Fisheries and Conservation Department): available at: http://www.afcd.gov.hk/ (last access: 21 January 2014), 2008.

AFCD (Agriculture, Fisheries and Conservation Department): Useful statistics, available at: http://www.afcd.gov.hk/english/country/cou_lea/cou_lea_use/cou_lea_use.html, last access: 2 June 2015.

Archibald, A. T., Khan, M. A. H., Watson, L. A., Utembe, S. R., Shallcross, D. E., Clemitshaw, K. C., and Jenkin, M. E.: Comment on "Long-term atmospheric measurements of C_1–C_5 alkyl nitrates in the Pearl River Delta region of southeast China" by Simpson et al., Atmos. Environ., 41, 7369–7370, 2007.

Arey, J., Aschmann, S. M., Kwok, E. S. C., and Atkinson, R.: Alkyl nitrate, hydroxyl nitrate, and hydroxycarbonyl formation from the NO_x-air photooxidations of C_5–C_8 n-alkanes, J. Phys. Chem., 105, 1020–1027, 2001.

Atkinson, R., Baulch, D. L., Cox, R. A., Crowley, J. N., Hampson, R. F., Hynes, R. G., Jenkin, M. E., Rossi, M. J., Troe, J., and IUPAC Subcommittee: Evaluated kinetic and photochemical data for atmospheric chemistry: Volume II – gas phase reactions of organic species, Atmos. Chem. Phys., 6, 3625–4055, doi:10.5194/acp-6-3625-2006, 2006.

Barletta, B., Meinardi, S., Simpson, I. J., Khwaja, H. A., Blake, D. R., and Rowland, F. S.: Mixing ratios of volatile organic compounds (VOCs) in the atmosphere of Karachi, Pakistan, Atmos. Environ., 36, 3429–3443, 2002.

Barletta, B., Meinardi, S., Simpson, I. J., Atlas, E. L., Beyersdorf, A. J., Baker, A. K., Blake, N. J., Yang, M., Midyett, J. R., Novak, B. J., McKeachie, R. J., Fuelberg, H. E., Sachse, G. W., Avery, M. A., Campos, T., Weinheimer, A. J., Rowland, F. S., and Blake, D. R.: Characterization of volatile organic compounds (VOCs) in Asian and north American pollution plumes during INTEX-B: identification of specific Chinese air mass tracers, Atmos. Chem. Phys., 9, 5371–5388, doi:10.5194/acp-9-5371-2009, 2009.

Bertman, S. B., Roberts, J. M., Parrish, D. D., Buhr, M. P., Goldan, P. D., Kuster, W. C., Fehsenfeld, F. C., Montzka, S. A., and Westberg, H.: Evolution of alkyl nitrates with air mass age, J. Geophys. Res., 100, 22805–22813, 1995.

Blake, N. J., Blake, D. R., Swanson, A. L., Atlas, E., Flocke, F., and Rowland, F. S.: Latitudinal, vertical, and seasonal variations of C_1–C_4 alkyl nitrates in the troposphere over the Pacific Ocean during PEM-Tropics A and B: Oceanic and continental sources, J. Geophys. Res., 108, 8242, doi:10.1029/2001JD001444, 2003.

Clemitshaw, K. C., Williams, J., Rattigan, O. V., Shallcross, D. E., Law, K. S., and Cox, R. A.: Gas-phase ultraviolet absorption cross-sections and atmospheric lifetimes of several C_2–C_5 alkyl nitrates, J. Photochem. Photobiol. A, 102, 117–126, 1997.

Gao, J., Wang, T., Ding, A. J., and Liu, C. B.: Observation study of ozone and carbon monoxide at the summit of mount Tai (1534 m a.s.l.) in central-eastern China, Atmos. Environ., 39, 4779–4791, 2005.

Guo, H., Jiang, F., Cheng, H. R., Simpson, I. J., Wang, X. M., Ding, A. J., Wang, T. J., Saunders, S. M., Wang, T., Lam, S. H. M., Blake, D. R., Zhang, Y. L., and Xie, M.: Concurrent observations of air pollutants at two sites in the Pearl River Delta and the implication of regional transport, Atmos. Chem. Phys., 9, 7343–7360, doi:10.5194/acp-9-7343-2009, 2009.

Guo, H., Cheng, H. R., Ling, Z. H., Louie, P. K. K., and Ayoko, G. A.: Which emission sources are responsible for the volatile organic compounds in the atmosphere of Pearl River Delta?, J. Hazard. Mater., 188, 116–124, 2011.

Guo, H., Ling, Z. H., Simpson, I. J., Blake, D. R., and Wang, D. W.: Observations of isoprene, methacrolein (MAC) and methyl vinyl ketone (MVK) at a mountain site in Hong Kong, J. Geophys. Res., 117, D19303, doi:10.1029/2012JD017750, 2012.

Guo, H., Ling, Z. H., Cheung, K., Jiang, F., Wang, D. W., Simpson, I. J., Barletta, B., Meinardi, S., Wang, T. J., Wang, X. M., Saunders, S. M., and Blake, D. R.: Characterization of photochemical pollution at different elevations in mountainous areas in Hong Kong, Atmos. Chem. Phys., 13, 3881–3898, doi:10.5194/acp-13-3881-2013, 2013a.

Guo, H., Ling, Z. H., Cheung, K., Wang, D. W., Simpson, I. J., and Blake, D. R.: Acetone in the atmosphere of Hong Kong: Abundance, sources and photochemical precursors, Atmos. Environ., 65, 80–88, 2013b.

HKCSD (Hong Kong Census and Statistics Department): Hong Kong Energy Statistics: Annual Report, available at: http://www.censtatd.gov.hk (last access: 18 August 2015), 2010.

HKEPD (Hong Kong Protection Department): Air Quality in Hong Kong, available at: http://www.epd-asg.gov.hk/api_history/english/report/files/AQR2012e_final.pdf (last access: 18 August 2015), 2012.

Jenkin, M. E. and Clemitshaw, C.: Ozone and other secondary photochemical pollutants: Chemical processes governing their for-

mation in the planetary boundary layer, Atmos. Environ., 34, 2499–2527, 2000.

Jenkin, M. E., Saunders, S. M., Wagner, V., and Pilling, M. J.: The tropospheric degradation of volatile organic compounds: A protocol for mechanism development, Atmos. Environ., 31, 81–107, 1997.

Jenkin, M. E., Saunders, S. M., Wagner, V., and Pilling, M. J.: Protocol for the development of the Master Chemical Mechanism, MCM v3 (Part B): tropospheric degradation of aromatic volatile organic compounds, Atmos. Chem. Phys., 3, 181–193, doi:10.5194/acp-3-181-2003, 2003.

Jiang, F., Guo, H., Wang, T. J., Cheng, H. R., Wang, X. M., Simpson, I. J., Ding, A. J., Saunders, S. M., Lam, S. H. M., and Blake, D. R.: An O_3 episode in the Pearl River Delta: field observation and model simulation, J. Geophys. Res., 115, D22305, doi:10.1029/2009JD013583, 2010.

Kwok, E. S. C. and Atkinson, R.: Estimation of hydroxyl radical reaction-rate constants for gas-phase organic-compounds using a structure-reactivity relationship-an update, Atmos. Environ., 29, 1685–1695, 1995.

Lam, S. H. M., Saunders, S. M., Guo, H., Ling, Z. H., Jiang, F., Wang, X. M., and Wang, T. J.: Modelling VOC source impacts on high ozone episode days observed at a mountain summit in Hong Kong under the influence of mountain-valley breezes, Atmos. Environ., 81, 166–176, 2013.

Ling, Z. H. and Guo, H.: Contribution of VOC sources to photochemical ozone formation and its control policy implication in Hong Kong, Environ. Sci. Pol., 38, 180–191, 2014.

Ling, Z. H., Guo, H., Cheng, H. R., and Yu, Y. F.: Sources of ambient volatile organic compounds and their contributions to photochemical ozone formation at a site in the Pearl River Delta, southern China, Environ. Pollut., 159, 2310–2319, 2011.

Ling, Z. H., Guo, H., Lam, S. H. M., Saunders, S. M., and Wang, T.: Atmospheric photochemical reactivity and ozone production at two sites in Hong Kong: Application of a Master Chemical Mechanism-photochemical box model, J. Geophys. Res.-Atmos., 119, 10567–10582, doi:10.1002/2014JD021794, 2014.

Lyu, X. P., Ling, Z. H., Guo, H., Saunders, S. M., Lam, S. H. M., Wang, N., Wang, Y., Liu, M., and Wang, T.: Re-examination of C_1–C_5 alkyl nitrates in Hong Kong using an observation-based model, Atmos. Environ., 120, 28–37, 2015.

Lyu, X. P., Ling, Z. H., Guo, H., Zeng, L. W., and Wang, N.: Impact of alkyl nitrate chemistry on photochemical reactivity and O_3 production in Hong Kong, in preparation, 2016.

Marandino, C. A., Tegtmeier, S., Krüger, K., Zindler, C., Atlas, E. L., Moore, F., and Bange, H. W.: Dimethylsulphide (DMS) emissions from the western Pacific Ocean: a potential marine source for stratospheric sulphur?, Atmos. Chem. Phys., 13, 8427–8437, doi:10.5194/acp-13-8427-2013, 2013.

Paatero, P.: User's guide for Positive Matrix Factorization Programs PMF2 and PMF3, part 1: Tutorial, prepared by University of Helsinki, Finland (February), 2000.

Pinho, P. G., Lemos, L. T., Pio, C. A., Evtyugina, M. G., Nunes, T. V., and Jenkin, M. E.: Detailed chemical analysis of regional-scale air pollution in western Portugal using an adapted version of MCM v3.1, Sci. Total Environ., 407, 2024–2038, 2009.

Reeves, C. E., Slemr, J., Oram, D. E., Worton, D., Penkett, S. A., Stewart, D. J., Purvis, R., Watson, N., Hopkins, J., Lewis, A., Methven, J., Blake, D. R., and Atlas, E.: Alkyl nitrates in outflow from North America over the North Atlantic during intercontinental transport of ozone and precursors 2004, J. Geophys. Res., 112, D10S037, doi:10.1029/2006JD007567, 2007.

Roberts, J. M., Bertman, S. B., Parrish, D. D., Fehsenfeld, F. C., Johnson, B. T., and Niki, H.: Measurements of alkyl nitrates at Chebogue Point Nova Scotia during the 1993 North Atlantic Regional Experiment (NARE) intensive, J. Geophys. Res., 103, 13569–13580, 1998.

Russo, R. S., Zhou, Y., Haase, K. B., Wingenter, O. W., Frinak, E. K., Mao, H., Talbot, R. W., and Sive, B. C.: Temporal variability, sources, and sinks of C_1–C_5 alkyl nitrates in coastal New England, Atmos. Chem. Phys., 10, 1865–1883, doi:10.5194/acp-10-1865-2010, 2010.

Saunders, S. M., Jenkin, M. E., Derwent, R. G., and Pilling, M. J.: Protocol for the development of the Master Chemical Mechanism, MCM v3 (Part A): tropospheric degradation of non-aromatic volatile organic compounds, Atmos. Chem. Phys., 3, 161–180, doi:10.5194/acp-3-161-2003, 2003.

Seinfeld, J. H. and Pandis, S. N.: Atmospheric Chemistry and Physics: from air pollution to climate change, 2nd Edn., Wiley Publisher, New Jersey, USA, 2006.

Simpson, I. J., Meinardi, S., Blake, D. R., and Blake, N. J.: A biomass burning source of C_1–C_4 alkyl nitrates, Geophys. Res. Lett., 29, 2168, doi:10.1029/2002GL016290, 2002.

Simpson, I. J., Blake, N. J., Blake, D. R., Atlas, E., Flocke, F., Crawford, J. H., Fuelberg, H. E., Kiley, C. M., Meinardi, S., and Rowland, F. S.: Photochemical production and evolution of selected C_2–C_5 alkyl nitrates in tropospheric air influenced by Asia outflow, J. Geophys. Res., 108, 8808, doi:10.1029/2002JD002830, 2003.

Simpson, I. J., Wang, T., Guo, H., Kwok, Y. H., Flocke, F., Atlas, E., Meinardi, S., Rowland, F. S., and Blake, D. R.: Long-term atmospheric measurements of C_1–C_5 alkyl nitrates in the Pearl River Delta region of southeast China, Atmos. Environ., 40, 1619–1632, 2006.

Simpson, I. J., Blake, N. J., Barletta, B., Diskin, G. S., Fuelberg, H. E., Gorham, K., Huey, L. G., Meinardi, S., Rowland, F. S., Vay, S. A., Weinheimer, A. J., Yang, M., and Blake, D. R.: Characterization of trace gases measured over Alberta oil sands mining operations: 76 speciated C_2–C_{10} volatile organic compounds (VOCs), CO_2, CH_4, CO, NO, NO_2, NO_y, O_3 and SO_2, Atmos. Chem. Phys., 10, 11931–11954, doi:10.5194/acp-10-11931-2010, 2010.

Simpson, I. J., Akagi, S. K., Barletta, B., Blake, N. J., Choi, Y., Diskin, G. S., Fried, A., Fuelberg, H. E., Meinardi, S., Rowland, F. S., Vay, S. A., Weinheimer, A. J., Wennberg, P. O., Wiebring, P., Wisthaler, A., Yang, M., Yokelson, R. J., and Blake, D. R.: Boreal forest fire emissions in fresh Canadian smoke plumes: C_1–C_{10} volatile organic compounds (VOCs), CO_2, CO, NO_2, NO, HCN and CH_3CN, Atmos. Chem. Phys., 11, 6445–6463, doi:10.5194/acp-11-6445-2011, 2011.

Sommariva, R., Trainer, M., de Gouw, J. A., Roberts, J. M., Warneke, C., Atlas, E., Flocke, F., Goldan, P. D., Kuster, W. C., Swanson, A. L., and Fehsenfeld, F. C.: A study of organic nitrates formation in an urban plume using a Master Chemical Mechanism, Atmos. Environ., 42, 5771–5786, 2008.

Talukdar, R. K., Burkholder, J. B., Hunter, M., Gilles, M. K., Roberts, J. M., and Ravishankara, A. R.: Atmospheric fate of several alkyl nitrates Part 2 UV absorption cross-sections and

photodissociation quantum yields, J. Chem. Soc. Faraday T., 93, 2797–2805, 1997.

Wang, M., Shao, M., Chen, W. T., Lu, S. H., Wang, C., Huang, D. K., Yuan, B., Zeng, L. M., and Zhao, Y.: Measurements of C_1–C_4 alkyl nitrates and their relationships with carbonyl compounds and O_3 in Chinese cities, Atmos. Environ., 81, 389–398, 2013.

Wang, T., Poon, C. N., Kwok, Y. H., and Li, Y. S.: Characterizing the temporal variability and emission patterns of pollution plumes in the Pearl River Delta of China, Atmos. Environ., 37, 3539–3550, 2003.

Wang, T., Wong, H. L. A., Tang, J., Ding, A., Wu, W. S., and Zhang, X. C.: On the origin of surface ozone and reactive nitrogen observed at a remote site in the northeastern Qinghai-Tibetan Plateau, western China, J. Geophys. Res., 111, D08303, doi:10.1029/2005JD006527, 2006.

Worton, D. R., Reeves, C. E., Penkett, S. A., Sturges, W. T., Slemr, J., Oram, D. E., Bandy, B. J., Bloss, W. J., Carslaw, N., Davey, J., Emmerson, K. M., Gravestock, T. J., Hamilton, J. F., Heard, D. E., Hopkins, J. R., Hulse, A., Ingram, T., Jacob, M. J., Lee, J. D., Leigh, R. J., Lewis, A. C., Monks, P. S., and Smith, S. C.: Alkyl nitrate photochemistry during the tropospheric organic chemistry experiment, Atmos. Environ., 44, 773–785, 2010.

Wu, Z. Y., Wang, X. M., Chen, F., Turnipseed, A. A., Guenther, A., Niyogi, D., Charusombat, U., Xia, B. C., Munger, J. W., and Alapty, K.: Evaluating the calculated dry deposition velocities of reactive nitrogen oxides and ozone from two community models over a temperate deciduous forest, Atmos. Environ., 45, 2633–2674, 2011.

Yuan, B., Liu, Y., Shao, M., Lu, S. H., and Streets, D. G.: Biomass burning contributions to ambient VOCs species at a receptor site in the Pearl River Delta (PRD), China, Environ. Sci. Technol., 44, 4577–4582, 2010.